RESEARCH PAPER

L-proline-linked N-GQDs/ZnO/CuO Chiral Retrievable Catalyst: Synthesis, Characterization, and Investigation of Catalytic Performance in Diastereoselective Synthesis of Furocoumarin Natural Products

Pouria Babaei, Javad Safaei-Ghomi*

Department of Organic Chemistry, Faculty of Chemistry, University of Kashan, Kashan, Iran

ARTICLE INFO

ABSTRACT

The advancement of nanocatalysts for chemical reaction progress in conjunction with the green chemistry parameters has been widely considered today. Graphene Quantum Dots (GQDs) have been extensively investigated due to their interesting photochemical, and electrochemical properties. Besides, heteroatom doping is a smart technique to adjust the catalytic properties of GQDs. Nitrogen-doped GQDs (N-GQDs) have rarely been introduced in the catalysis field. Therefore, we proposed a hydrothermal route for the straightforward fabrication of N-GQDs/ ZnO/CuO heterojunction nanocomposites as an efficient nanocatalyst. Also, L-proline-linked N-GQDs/ZnO/CuO nanocomposites as a chiral retrievable catalyst in the synthesis of diastereoselective three-component reactions (4-bromophenacyl bromide, aromatic aldehydes, and 4-hydroxycoumarin) to afford of furocoumarins natural product. According to the obtained results, various parameters such as solvent, temperature, and pH range could control the nanocatalyst morphology. In the following, the catalytic activity of engineered heterojunction nanocomposite was screened in the one-pot diastereoselective synthesis of new and known furocoumarin derivatives natural product. During the three-component reaction progress, three new sigma bonds (two C-C and one C-O) were formed which led to the formation of the products in excellent yields (86-96 %) in a short time. Also, to achieve the highest catalytic efficiency, the influence of main parameters such as temperature, solvent, and the molar ratio of the nanocomposites were optimized. High diastereoselectivity, good to excellent atom economy, very short reaction time (35 min), reusability of catalyst (7 times), and a bit catalyst loading can be cited as the other notable features of this strategy.

INTRODUCTION

Graphene quantum dots (GQDs), which are a unique fellow of carbon nanomaterials [1] have been revealed splendid attributes such as excellent biocompatibility [2], emission, low cytotoxicity [3], extremely soluble in various solvents [4], and photoluminescence (PL) [5]. Due to high specific surface area and functional groups rich surface (–OH, -CO₂H, etc.), GQDs are capable of strong interaction with nanocomposites and also, GQDs carry various chiral small-molecules as chemical catalysts [6, 7]. Therefore GQDs are referred to as

* *Corresponding Author Email: safaei@kashanu.ac.ir*

remarkable "linkers" in metal-organic framework catalysts (MOFs) [8]. Heteroatom doping such as nitrogen, phosphorus, and sulfur atom gives rise to the unique chemical properties of GQDs, such as low toxicity, strong absorption, excellent solubility, good biocompatibility, and catalysts. Besides, Nitrogen-doped GQDs (N-GQDs) is a great electron transfer carrier. Also, N-GQDs provide more active sites, leading to their more effective and applied application for catalytic performance [9, 10]. Nano-size zinc oxide (ZnO) affords some benefits, for instance, low price, high surface area, eco-friendly, and high electron mobility [11]. Nowadays, various approaches have been developed to the fabrication of new ZnO-based nanostructures concerning catalytic activities [12]. Among them, ZnO/CuO heterojunction nanocomposites attracted much attention from investigators because of their different applications such as catalyst in organic synthesis, solar cell, and photocatalyst [13, 14]. However, the fabrication of N-GQDs/ZnO/CuO heterojunction nanocomposites has rarely been investigated as nanocatalysts in organic reactions [15]. Thus, we intend to develop the N-GQDs/ZnO/CuO heterojunction nanocomposites via a simple route entailing one-pot fabrication of ZnO/CuO nanorod and then hydrothermal treatment to get the final nanocatalyst.

Pristine L-proline has been accredited as a significant chiral small-molecule organocatalyst [16]. Due to its easy availability [17], ecological and accessible in two enantiomeric forms [18], it has been paid much attention in the preparation of organic compounds as a catalyst via multicomponent reactions (MCRs) [19, 20]. However, L-proline-mediated gives poor stereoselectivity, long-term completion process, and difficult reusability in asymmetric reactions [21]. Using some strategies such as the addition of additives [22], co-catalysts [23], various types of support like polymers [24], silica [25], ionic liquid (IL) [26], and MOFs [27] could also help to resolve these restrictions. For example, Kaskel [28], Bae [29], and Zou [30] used L-proline as a functionalized and supporting catalyst in asymmetric Michael addition, asymmetric aldolization, and diastereoselective aldol reactions, respectively. In general, many research papers have been published since the last decade on the role of L-proline as a chiral catalyst [25].

Furocoumarins, which belong to an extraordinary category of heterocyclic compounds, present in countless natural products [31]. Additionally, they have a wide spectrum of biological properties, for instance, antifungal [32], anticancer [33], antibacterial, vasorelaxant [34], inhibition of human CYP 1B1 isoform [35], and HIV-1 integrase inhibitors [36]. Many methods for the synthesis of furocoumarins have been expanded in recent years owing to their ecological and medicinal importance [37]. Multicomponent reactions (MCRs) are one of the powerful strategies for the preparation of furocoumarins in the presence of various catalysts, for example, 4-dimethylaminopyridine (DAMP) [38], a combination of AcOH/AcONH$_4$ [39], ionic liquid [BMIm]OH [40], Pd(CF$_3$CO$_2$)$_2$ [41], I$_2$/K$_2$S$_2$O$_8$ [42], N-methylimidazolium and triethylamine [43]. A number of these procedures have particular disadvantages such as prolong completion time, usage of toxic materials, non-reusable catalysts, and special usage conditions.

Herein, we set a facile one-pot reaction of 4-bromophenacyl bromide, various aryl aldehydes, and 4-hydroxycoumarin to afford furocoumarins using L-proline-linked N-GQDs/ZnO/CuO nanocomposites (Fig. 1). Taken together, we disclose our comprehensive research of the stereochemistry, mechanism of the reaction, and chiral organometallic catalyst interaction.

MATERIALS AND METHODS
Apparatus and materials

All melting points were determined by an Electro-Thermal 9200 and are uncorrected. FT-IR spectra of all compounds were recorded on Nicolet Magna 550 IR spectrometer using KBr pellets in the range of 400–4000 cm^{-1}. ^{1}H and ^{13}C NMR spectra were measured by a Bruker 400 MHz spectrometer at 400 and 100 MHz, respectively. TMS as an internal reference and were carried out using CDCl$_3$ as an NMR spectroscopy solvent. XRD pattern was performed on a Philips diffractometer using monochromatized Cu Kα radiation (k = 1.5406 Å). Elemental analyses (C, H, and N) were recorded using a Carlo ERBA analyzer (model EA1108). FE-SEM images of products were imagined by an LEO instrument (model 1455VP). The morphology and size distribution of N-GQDs/ZnO/CuO heterojunction nanocomposites were taken by High-resolution transmission electron microscopy (HRTEM, FEI Tecnai F20). The entire experiments in this research were purchased in
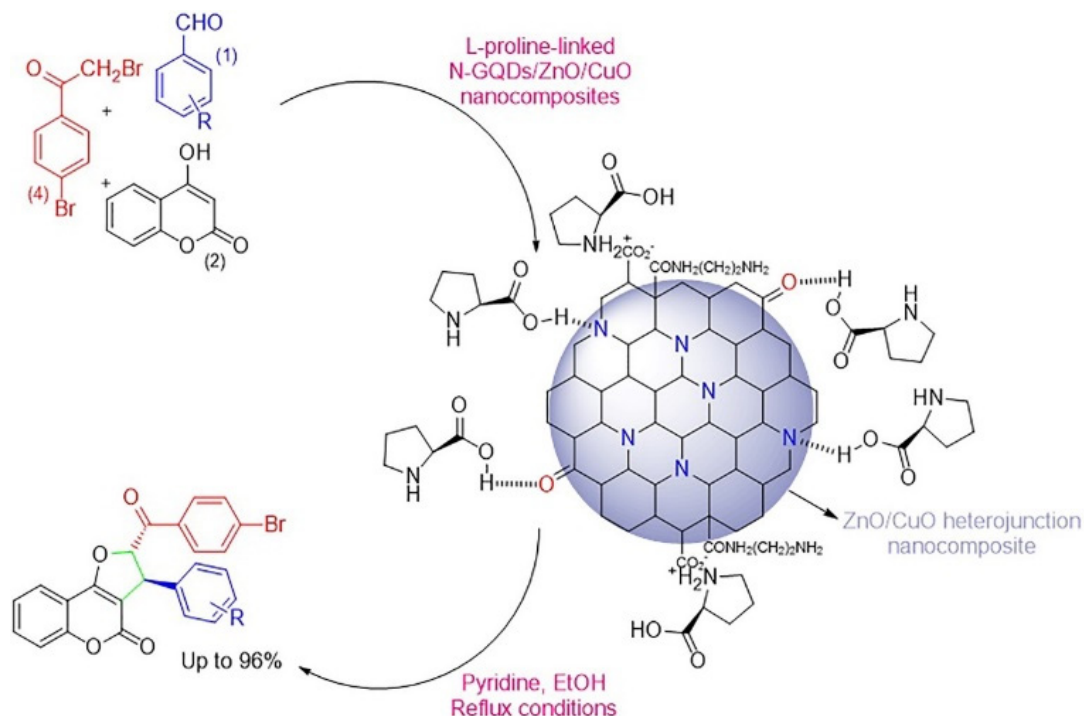
Fig. 1. L-proline-linked N-GQDs/ZnO/CuO heterojunction nanocomposite as a chiral retrievable catalyst in the diastereoselective synthesis of furocoumarins natural product.

Table 1. Various hydrothermal conditions of fabrication of ZnO/CuO heterojunction nanocomposites in pH=12.

No.	Mole ratio (Cu^{2+}:Zn^{2+})	Temperature (°C)	Time (h)	Shape
1	1:1	120	12	Nano coral
2	1:1	150	12	nanospheres
3	1:1	180	12	heterojunction structures
4	1:2	180	12	nanorods/nanospheres
5	2:1	180	12	nanocluster
6	1:1	180	10	nanospheres
7	1:1	180	14	nanorods/nanospheres

analytical grade from Merck and Sigma-Aldrich without extra purification.

Fabrication of ZnO/CuO heterojunction nanocomposites.

Copper (II) acetate (0.6 g) and zinc (II) acetate (0.66 g) were dissolved separately in ultrapure water (20 ml) at room temperature. Next, the zinc solution was added drop by drop to the copper solution. Then, NaOH (1 g) was dissolved in ultrapure water (10 ml), later was added to the above mixture with stirring. The mixture was stirred for 15 min at room temperature and then, put into a Teflon-lined stainless steel autoclave under various hydrothermal conditions (Table 1). The black sediment was firstly centrifuged and followed by washing with distilled water several

times. The obtained precipitate was dried at 65 °C and calcined at 500 °C for 2 h.

$$Cu(CH_3CO_2)_2 + Zn(CH_3CO_2)_2 + 4\ NaOH \rightarrow ZnO/CuO + 4\ NaCH_3CO_2 + 4\ H_2O$$
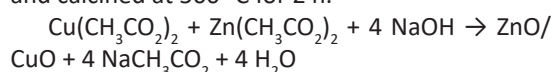
Fabrication of N-GQDs/ZnO/CuO heterojunction nanocomposites.

Ethylenediamine (0.5 ml), citric acid (1.2 g), and ultrapure water (50 ml), initially, were stirred for 2 min at room temperature. Next, ZnO/CuO heterojunction nanocomposites (1 g) were added to the above solution and stirred for another 2 min. Then the mixture was put into a 100 ml Teflon-lined stainless steel autoclave. The sealed autoclave was placed on an electric oven under 180°C for 10 h. N-GQDs/ZnO/CuO nanocomposites were collected by centrifugation at 10000 rpm for

15 min. The dark brown precipitate was dried at 60°C for 24 h under vacuum conditions.

Fabrication L-proline-linked N-GQDs/ZnO/CuO nanocomposites.

N-GQDs/ZnO/CuO nanocomposites (1 g) and L-proline (1.6 g) were dissolved in 15 ml dry toluene and stirred, followed by heating at reflux conditions for an appropriate time. Then, the obtained solid was centrifuged and washed with absolute ethanol three times. The purified precipitate was finally dried overnight at 40°C.

General method for the preparation of furo[3,2,c] coumarins.

To a mixture of pyridine (1.0 mmol) and 4-bromophenacyl bromide (1.0 mmol) in ethanol, was added proper aryl aldehyde (1.0 mmol), 4-hydroxycoumarin (1.0 mmol), L-proline-linked N-GQDs/ZnO/CuO nanocomposites as a chiral retrievable nanocatalyst, and stirred under reflux conditions. The completion of the reaction was determined by TLC analysis. After the end of the reaction, the crude mixture was filtered and washed by cold EtOH.

Physical and spectroscopic data of new and selected products.

2.6.1. trans-2-(4'-bromo-benzoyl)-3-(4-nitrophenyl)-2H-furo[3,2-c]chromen-4(3H)-one *(5b):* White powder, m.p 251-253 ºC, IR (KBr) cm^{-1}: 2919, 2841, 1724, 1644, 1456,1407, 1029, 754, 574; ^{1}H NMR (400 MHz, DMSO-d_6): δ (ppm) 5.13 (CH, 1H, J= 5.2 Hz), 6.05 (CH, 1H, J= 5.2 Hz), 7.27-7.29 (m, 2H), 7.30 (t, J = 7.2 Hz, 1 H), 7.41- 7.44 (m, 1H), 7.45 (d, J = 7.6 Hz, 2H), 7.48 (d, J = 7.6 Hz, 2H) 7.91- 8.11 (m, 4H); ^{13}C NMR (100 MHz, CDCl$_3$): δ (ppm) 47.98, 92.01, 103.97, 112.04, 116.97, 122.97, 123.95, 125.01, 127.99, 130.34, 131.02, 132.04, 133.03, 133.65, 145.96, 148.02, 156.10, 160.04, 165.98, 191.01; Anal. calcd for $C_{24}H_{14}BrNO_6$: C, 58.56; H, 2.87; N, 2.85; Found: C, 58.49; H, 2.78; N, 2.82; $[\alpha]^{22}_D$ = +17.49 (c 0.13, CHCl$_3$).

trans-2-(4'-bromo-benzoyl)-3-(2-fluorophenyl)-2H-furo[3,2-c]chromen-4(3H)-one *(5f)*: White powder, m.p 187-188º C, IR (KBr) cm^{-1}: 3065, 2977, 1713, 1647, 1492, 1408, 1049, 766, 501; ^{1}H NMR (400 MHz, CDCl$_3$): δ (ppm) 5.17 (CH, 1H, J = 5.2 Hz), 6.13 (CH, 1H, J = 5.2 Hz), 7.10 (d, $^3J_{FH}$= 8.8Hz, 1H), 7.25-7.52 (m, 5H), 7.48-7.50 (m, 3H), 7.51 (d, J= 7.6 Hz, 1H), 7.97-8.01 (m, 2H);

^{13}C NMR (100 MHz, CDCl$_3$): δ (ppm) 47.97, 91.96, 104.99, 114.42, 116.94, 123.14, 123.25, 123.36, 123.39, 124.17, 124.29, 129.43, 130.07, 130.56, 130.90, 130.98, 132.47, 132.79, 133.19, 162.22 (d, F-C, ^1J=118.8 Hz, 1C), 162.37, 190.95; Anal. calcd for $C_{24}H_{14}BrFO_4$: C, 61.96; H, 3.03; Found: C, 61.81; H, 2.90; $[\alpha]^{22}_D$ = +48.02 (c 0.3, CHCl$_3$).

trans-2-(4'-bromo-benzoyl)-3-(4-methylthiophenyl)-2H-furo[3,2-c]chromen-4(3H)-one *(5g):* White powder, m.p 205-207 ºC, IR (KBr) cm^{-1}: 2926, 2840, 1727, 1641, 1494, 1025, 757, 540; ^{1}H NMR (400 MHz, CDCl$_3$): δ (ppm) 2.66 (s, CH$_3$, 3H), 4.77 (CH, 1H, d, J= 4.8 Hz), 6.07 (CH, 1H, d, J= 4.8 Hz), 7.16-7.27 (m, 4H), 7.30-7.33 (m, 1H), 7.41-7.87 (m, 7H); ^{13}C NMR (100 MHz, CDCl$_3$): δ (ppm) 14.98, 49.12, 91.97, 105.12, 111.97, 116.91, 121.03, 121.94, 125.08, 126.18, 126.97, 127.94, 129.14, 131.89, 132.89, 135.24, 140.14, 156.41, 160.16, 167.18, 191.04. Anal. calcd for $C_{25}H_{17}BrO_4S$: C, 60.86; H, 3.47; Found: C, 60.73; H, 3.55; $[\alpha]^{22}_D$ = +41.20 (c 0.5, CHCl$_3$).

Recycling of L-proline-linked N-GQDs/ZnO/CuO heterojunction nanocomposites

To recycle catalyst, the obtained solid was dissolved in CHCl$_3$ (nanocatalyst was not dissolved in CHCl$_3$). Subsequently, it could be collected by centrifuge at a speed of 12000 rpm for 6 min and dried at 65° C for 8h.

RESULTS AND DISCUSSION
Structural characterization of nanocatalyst

The hydrothermal method has been widely applied by most investigators due to its cheap, eco-friendly, and low-cost pathway. [44]. Also, this procedure allows for controlling the size and morphology of the nanostructures by using various reaction conditions [45]. Fig. 2 demonstrates the successful synthesis of L-proline-linked N-GQDs/ZnO/CuO heterojunction nanocomposites during the hydrothermal route step by step.

FT-IR measurement (Fig. 3) was conducted to recognize more evidence for the surface functional groups of catalysts at each step. The peaks at 770 cm^{-1} and 580 cm^{-1} correspond to the vibrational absorption of Cu-O and Zn-O, respectively (Fig. 3a). Fig. 3b shows the attendance of O-H (strong and broadened at 3410 cm^{-1}), C=O (1655 cm^{-1}), C=C $_{aromatic}$ (1551-1450 cm^{-1}), and C-N (1217 cm^{-1}), which confirm that N-GQDs has covered the core of the nanocomposites. From Fig. 3c, it is obvious that new bands at 1042 cm^{-1}, 1265 cm^{-1}, 1626

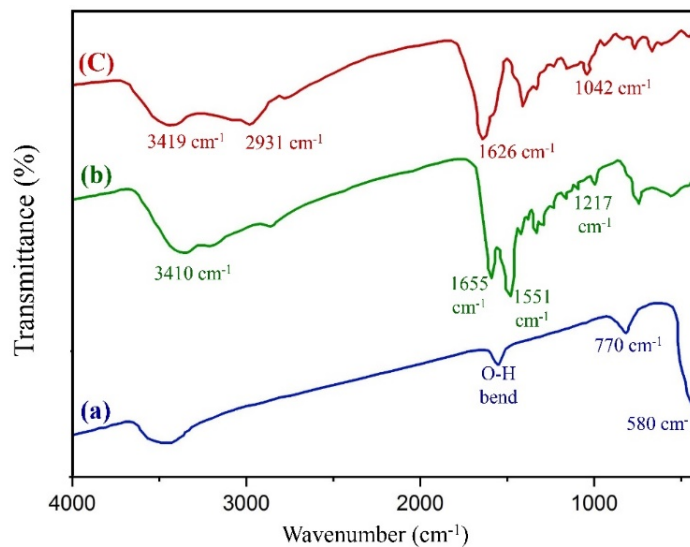Fig. 2. Schematic procedure of L-proline-linked N-GQDs/ZnO/CuO nanocomposites.

Fig. 3. The comparative FT-IR spectra of a) CuO/ZnO heterojunction nanocomposites, b) N-GQDs/ZnO/CuO nanocomposites, and c) L-proline-linked N-GQDs/ZnO/CuO nanocomposites.

cm^{-1}, 2931 cm^{-1}, and 3419 cm^{-1} are related to the stretching C-N, C-O, C=O, C-H (sp^3), and OH groups, respectively.

Fig. 4 reveals the XRD graph of L-proline-linked N-GQDs/ZnO/CuO nanocomposites. The diffraction angles (2Theta) for CuO are 36.61°, 39.15°, 49.22°, and 58.5° and also the diffraction angles (2Theta) for ZnO include 32.05°, 34.72°, 36.54°, 47.33°, 56.87°, 61.83°, 63.45°, 66.23°, 68.18°, 73.13°, and 75.48°, which corresponds
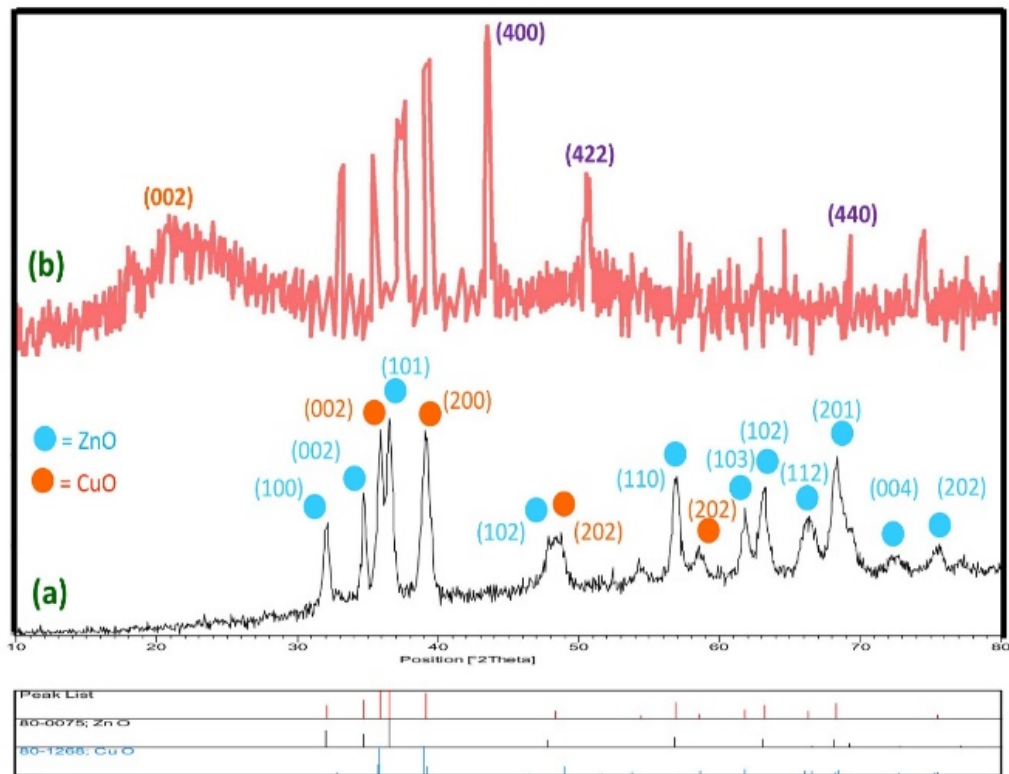
Fig 4. XRD patterns for a) ZnO/CuO heterojunction nanocomposites obtained at 180°C for 12 h, b) L-proline-linked N-GQDs/ZnO/CuO heterojunction nanocomposite.

to standard CuO and ZnO XRD patterns (JCPDS card No. 80-1268 and 80-0075, respectively). Miller indices for ZnO/CuO heterojunction nanocomposites are attached in Fig. 4a. The as-prepared nanocomposites have only two crystalline phases related to ZnO and CuO. Also, sharp peaks describe their high crystallinity. Crystallite sizes were calculated from Scherrer equation (Dc= Kλ/(βCosθ)), K is a dimensionless shape factor, which ordinarily takes a value of approximately 0.9, λ also is the X-ray wavelength (0.156 nm for CuKα radiation) and where β is the line broadening at half the maximum intensity (FWHM), was about 32 nm for ZnO/CuO heterojunction nanocomposites. Besides, it can be seen that a broad peak in the 2θ = 22°corresponding to (002) plane confirms the formation of a very tiny carbogenic core in N-GQDs [46]. The peaks obtained at 2θ = 44.1°, 52.9°, and 74.3° relating to (400), (422), and (440) planes, respectively, shows that the crystalline structure of the L-proline-linked N-GQDs/ZnO/CuO nanocomposite is formed (Fig. 4b) [47].

EDS spectroscopy was applied for the inquiry

purity of ZnO/CuO heterojunction nanocomposites (Fig. 5). The results of EDS analysis confirmed the existence of oxygen (51.61 w/w %), copper (35.55 w/w %), and zinc (13.04 w/w %) atoms in the structure (Fig. 5a). Furthermore, the presence of L-proline on the surface of N-GQDs/ZnO/CuO nanocomposite was proved with the appearance of C (40.47%) and N (21.10%) in the EDX spectrum (Fig. 5b).

GQDs are few-atoms-thick graphenes and their sizes are less than 30 nm [48]. AFM image demonstrates the topographic height of N-GQDs/ZnO/CuO heterojunction nanocomposites (Fig. 6). From the AFM image and its profile, the height of the proposed catalyst was lower than 19 nm.

The thermal stability of the catalyst is one of the most important factors in the recovery and reuse of catalyst [49]. For the investigation of the thermal stability, TG analysis was applied on a Mettler TG50 analyzer under continuous N_2 flow at a heating rate of 10 °C.min^{-1} in the range 30-800 °C. Thermal analysis of as-fabricated L-proline-linked N-GQDs/ZnO/CuO nanocomposites was presented
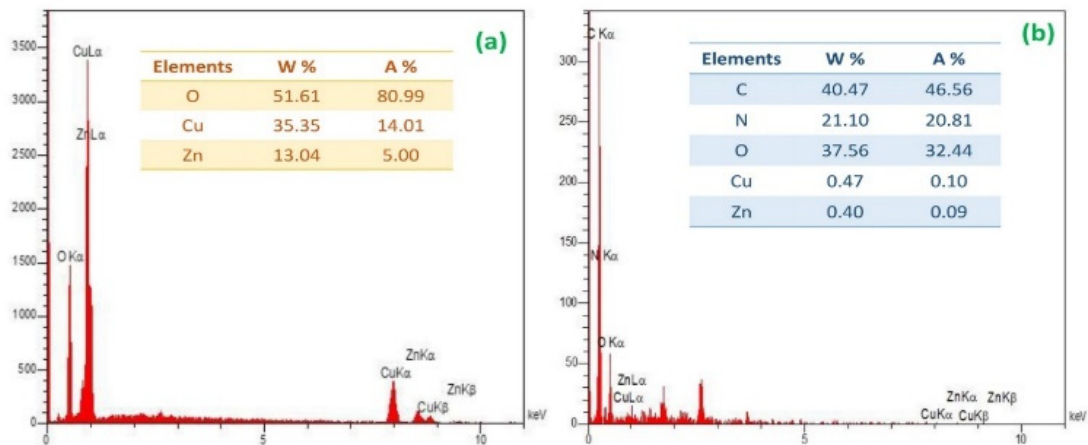
Fig. 5. EDS spectrum of a) ZnO/CuO heterojunction nanocomposites, b) L-proline-linked N-GQDs/ZnO/CuO nanocomposites.
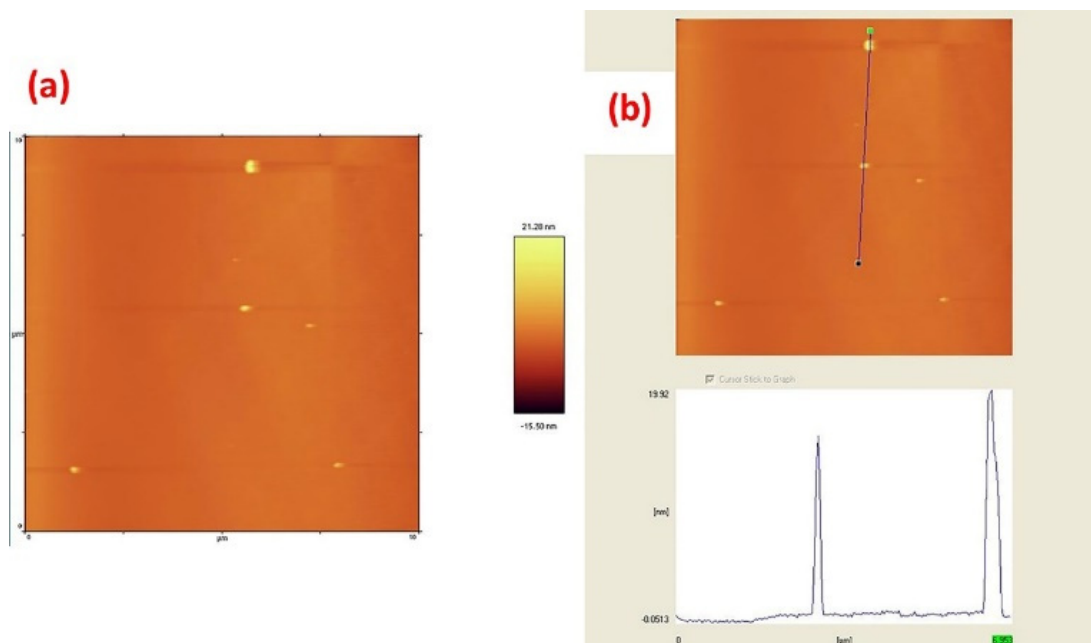

Fig. 6. (a) AFM image of N-GQDs/ZnO/CuO nanocomposites, and (b) the profile along the line in (a)

in Fig. 7. A 4% diminish in weight between 50 and 100°C is due to losing surface hydroxyl groups or solvent retained on the outside of the surface. A 48% decline in weight between 100 and 550°C is due to losing absorbed solvent molecules trapped in the N-GQDs layer and decomposition products of the L-proline functionalization.

Temperature, reaction time, and mole ratio are effective on the morphology and particle size [50]. Scanning electron microscope (SEM) analysis was utilized to investigate the ZnO/CuO heterojunction nanocomposite surface morphology. Fig. 8 demonstrates FE-SEM images of the as-fabricated ZnO/CuO heterojunction nanocomposites obtained in a 1:1 ratio (Cu^{2+}:Zn^{2+}), at 12 h, and various temperature. It shows ZnO/CuO heterojunction nanostructures with an average diameter size of less than 60 nm were prepared at 180°C (Fig. 8c). FE-SEM images reveal the coral-like and sphere-shaped morphology of ZnO/CuO (1:1) at 120°C and 150°C, respectively (Fig. 8, (a and b)).

From Fig. 9a and 9b become clear that morphology changed to nanorods/nanocluster
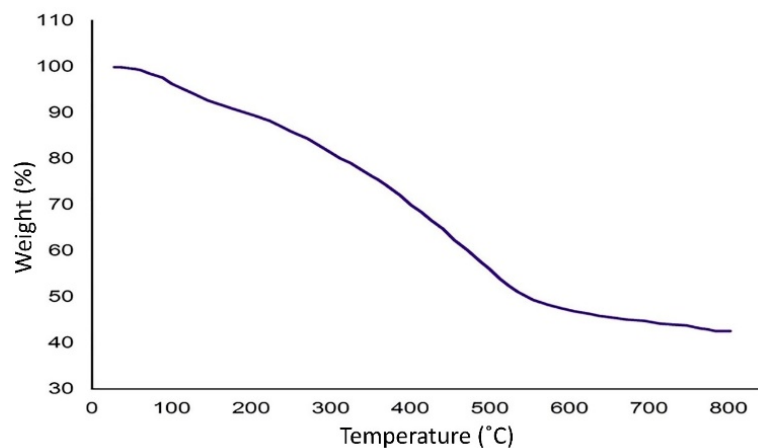
Fig. 7. TG analysis of L-proline-linked N-GQDs/ZnO/CuO heterojunction nanocomposites.
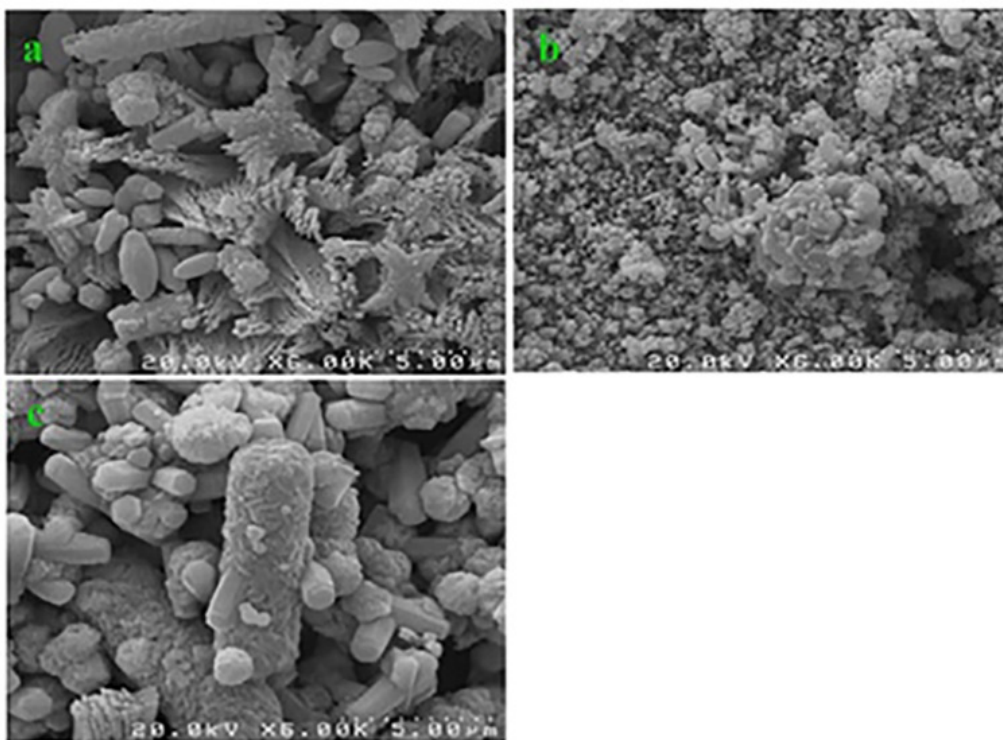

Fig. 8. FE-SEM images of ZnO/CuO heterojunction nanocomposites in a 1:1 mole ratio at 12 h, and a) 120°C, b) 150°C, c) 180°C.

(Cu^{2+}: Zn^{2+} = 1: 2), and nanocluster (Cu^{2+}: Zn^{2+} = 2: 1) at 180°C and 12 h, respectively. According to the previous FE-SEM images, it was found that the optimized conditions were 180 °C in a 1:1 ratio (Cu^{2+}:Zn^{2+}) (Fig. 9c).

The effect of time on morphological change was shown in Fig. 10. Fig. 10a and 10b display the various type of ZnO/CuO nanocomposites (nanosphere and nanorods/nanosphere) in 10 and

14 hours, respectively. From Fig. 10c, the optimized reaction time is found to be 12 h. FE-SEM images of as-prepared L-proline-linked N-GQDs/ZnO/CuO nanocomposites were presented in Fig. 11.

Furthermore, for better estimation of the morphology and size of nanocomposites were presented by transmission electron microscope (TEM) and high-resolution TEM (HRTEM) images. TEM (Fig.12 a) and HRTEM images (Fig. 12 (b-d))
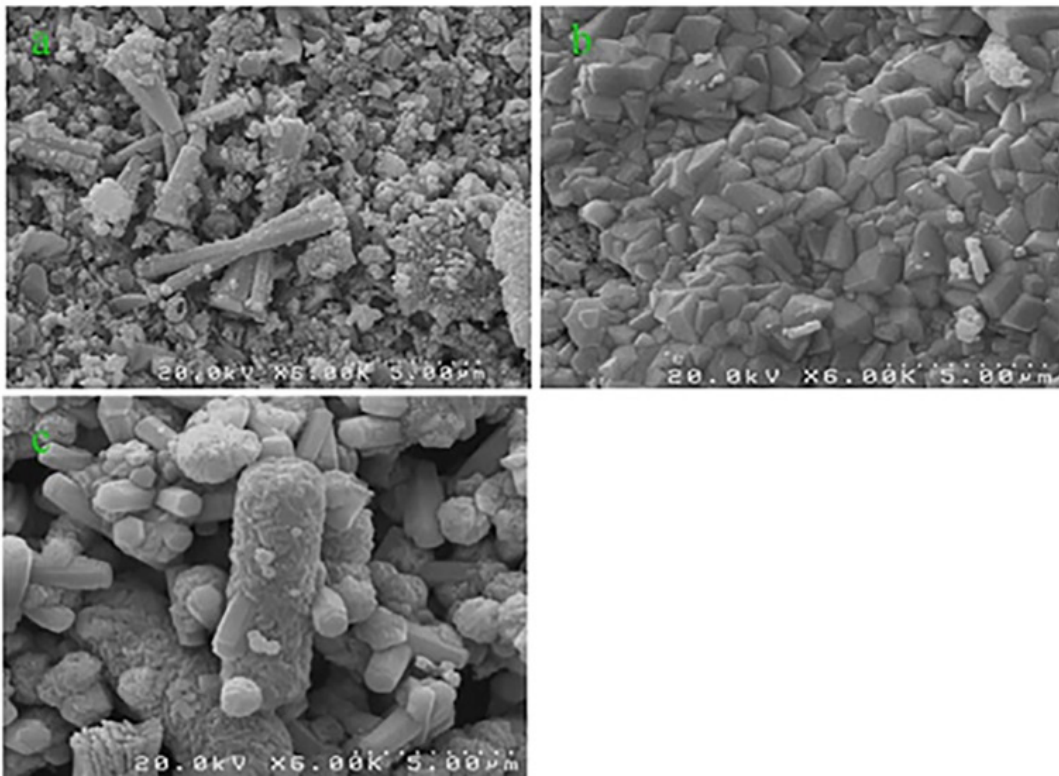
Fig. 9. FE-SEM images of ZnO/CuO heterojunction nanocomposites, at 180 °C and 12 h, the mole ratio of Cu^{2+}: Zn^{2+}, a) 1:2, b) 2:1, c) 1:1.
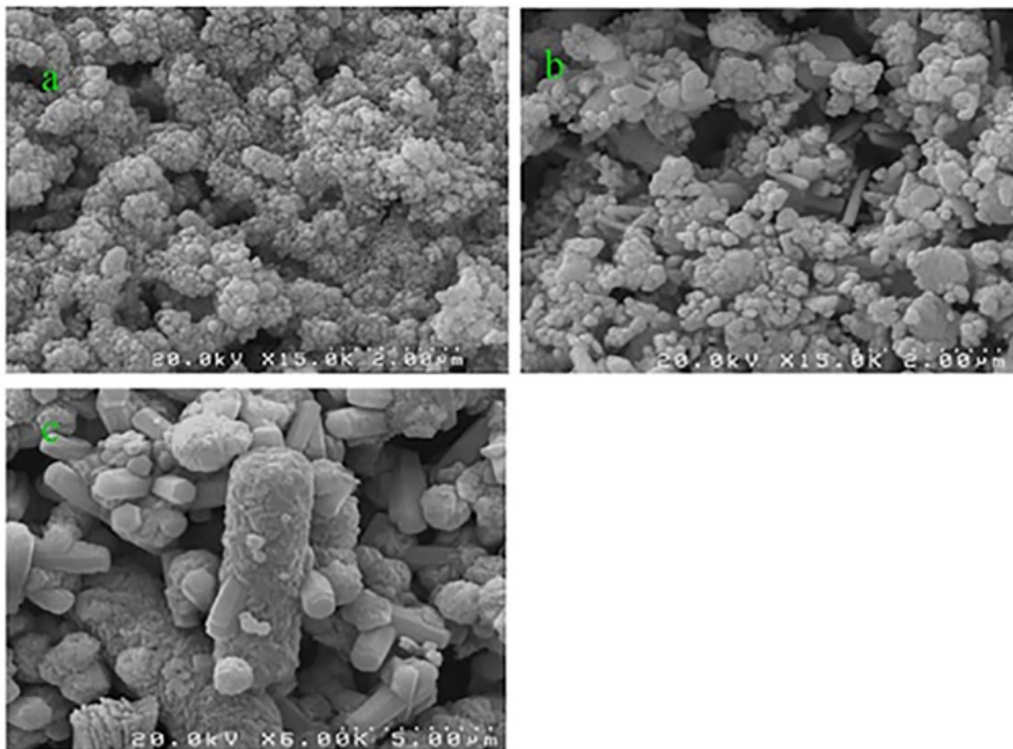

Fig. 10. FE-SEM images of ZnO/CuO heterojunction nanocomposites in a 1:1 mole ratio and 180 °C, a) 10 h, b) 14 h, c) 12 h.
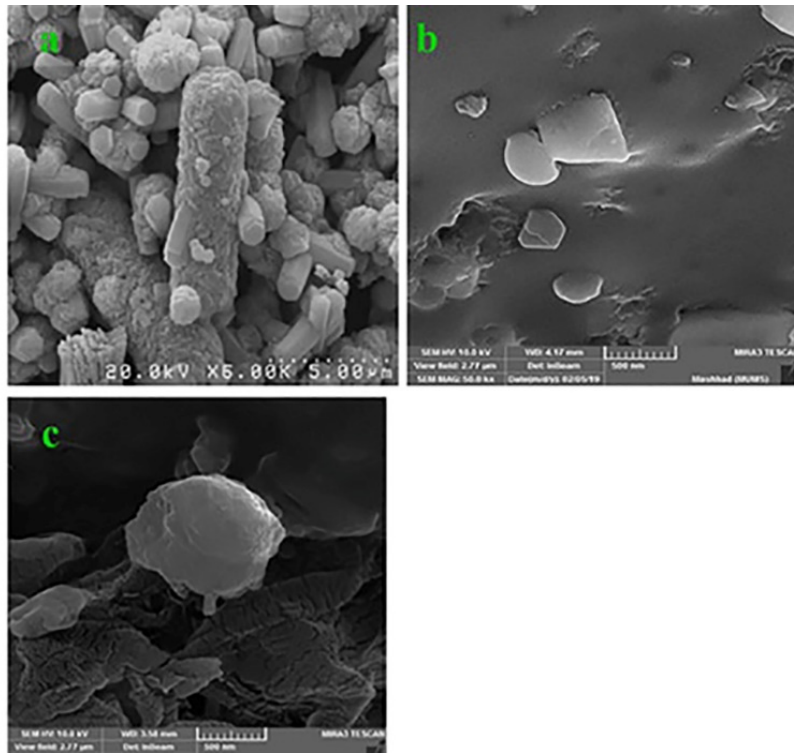
Fig. 11. FE-SEM images of a) ZnO/CuO heterojunction nanocomposites, b) N-GQDs/ZnO/CuO nanocomposites, c) L-proline-linked N-GQDs/ZnO/CuO nanocomposites.
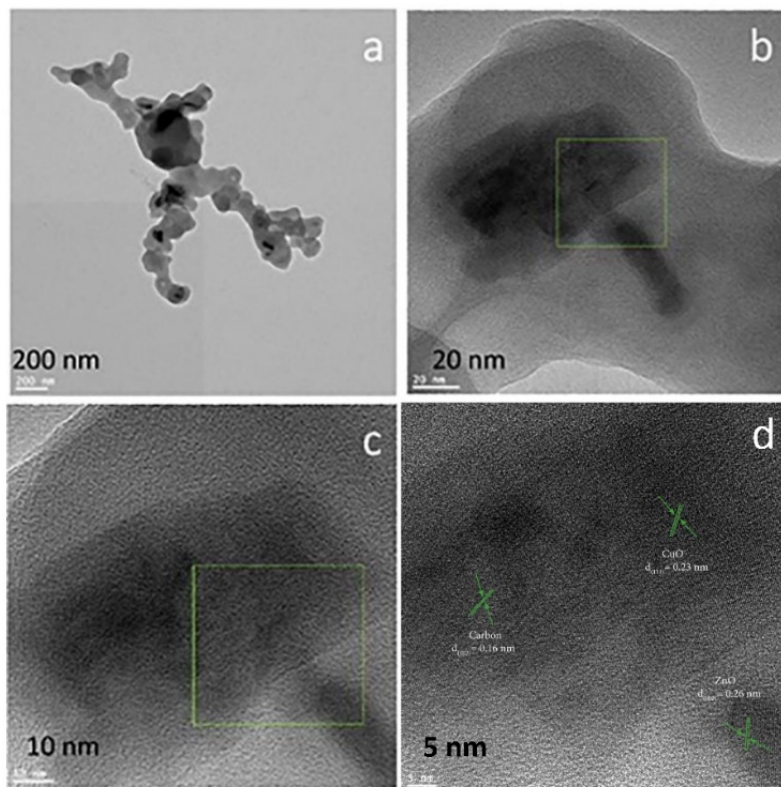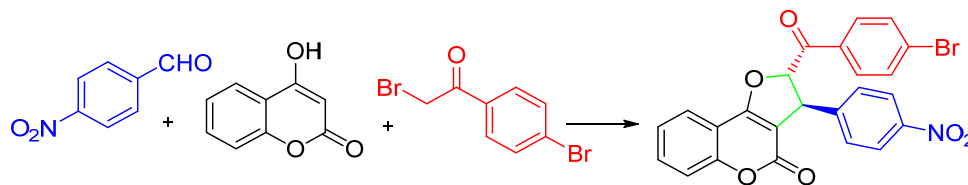

Fig. 12. (a) TEM image and (b-d) HRTEM of N-GQDs/ZnO/CuO nanocomposites.

Table 2. Optimization of reaction conditions using various solvents, catalysts, and catalyst loading on model reaction.

No.	Solvent	Catalyst (amount)	Time (min)	Yield (%)[b]
1	EtOH	----	180	< 5
2	EtOH	NEt₃ (10 mol%)	150	40
3	CH₃CN	NEt₃ (10 mol%)	180	26
4	EtOH	DMF (10 mol%)	210	22
5	CH₃CN	DMF (10 mol%)	250	18
6	EtOH	ZnO NPs (0.05 g)	170	36
7	EtOH	CuO NPs (0.08 g)	130	38
8	EtOH	N-GQDs (0.06 g)	140	33
9	EtOH	L-proline (0.1 g)	120	74
10	EtOH	ZnO/CuO nanocomposite (0.02 g)	110	48
11	EtOH	N-GQDs/ZnO/CuO nanocomposite (0.015 g)	100	51
12	H₂O	L-proline-linked N-GQDs/ZnO/CuO (0.013 g)	85	55
13	DMF	L-proline-linked N-GQDs/ZnO/CuO (0.013 g)	35	61
14	CH₃CN	L-proline-linked N-GQDs/ZnO/CuO (0.013 g)	35	71
15	EtOH	L-proline-linked N-GQDs/ZnO/CuO (0.013 g)	35	96
16	EtOH	L-proline-linked N-GQDs/ZnO/CuO (0.010 g)	35	88
17	EtOH	L-proline-linked N-GQDs/ZnO/CuO (0.015 g)	35	96

[a] Reaction condition: 4-nitrobenzaldehyde (1 mmol), 4-hydroxycoumarin (1 mmol), and phenacyl bromide (1 mmol) in the presence of L-proline-linked N-GQDs/ZnO/CuO nanocomposites.
[b] Isolated yield

indicated that the as-prepared nanocomposites were crystalline with a lattice spacing of 0.23, 0.26, and 0.16 nm which correspond to the (111) CuO (JCPDS file NO. 80-1268), (002) ZnO (JCPDS file NO. 80-0075) and (002) planes of graphitic carbon (JCPDS file no. 01-0646), respectively.

Catalytic study of L-proline-linked N-GQDs/ZnO/CuO nanocomposite as a chiral retrievable catalyst in the diastereoselective synthesis of furocoumarins natural products

It is noteworthy to mention that designing the appropriate conditions (e.g. modified chiral catalyst, temperature, etc.) could be effective in advancing the reaction and stereochemistry [51]. Hence, we start our job with the reaction between various aryl aldehyde (**1**), 4-hydroxycoumarin (**2**), pyridine (**3**), phenacyl bromide (**4**) (in a molar ratio), and a sufficient amount of chiral nanocatalyst via MCRs at reflux conditions for an appropriate time. Several reactions were tested using different solvents (e.g. water, acetonitrile, dimethylformamide, and ethanol). Ethanol is a green solvent and the reaction gave satisfying results when ethanol was used as a solvent (see Table 2).

During our investigation, we observed that the yield was lower than 5% in the absence of a catalyst. Also, results proved these catalysts were not suitable for stereoselectivity and the yield of the reaction was moderate (Table 2, entries 1-11). In contrast, when the reaction was carried out in attendance of L-proline-linked N-GQDs/ZnO/CuO nanocatalyst surprisingly good yield was achieved in less time (Table 2, entries 12-15). Moreover, the synthesis of furocoumarins was hitherto carried out in the presence of diverse catalysts. From Table 2 (entries 15-17), when 0.01, 0.013, and 0.015 g of L-proline-linked N-GQDs/ZnO/CuO nanocomposites were tested, the yield was 88, 96, and 96%, respectively. Consequently, 0.013 g of L-proline-linked N-GQDs/ZnO/CuO nanocomposites were suitable, and an excessive amount of catalyst did not alter the yields. Furocoumarins have been hitherto prepared in presence of various catalysts. Some of them are listed in Table 3.

As shown in Table 2, a comparative study was performed between synthesized L-proline-linked N-GQDs/ZnO/CuO nanocomposite and previously reported catalysts for the synthesis of furocoumarins. The use of L-proline (as catalyst

Table 3. A comparison study of L-proline-linked N-GQDs/ZnO/CuO nanocomposites with other catalysts and procedures for the synthesis of furocoumarins.

No.	Catalyst [Ref.]	Conditions	Time	Yield (%)
1	NEt₃[55]	CH_3CN/ reflux	2 h	81
2	TBAB[44]	H_2O/ 70 °C	3 h	83
3	[BMIn]OH[32]	CH_3CN/ 80 °C	1.5 h	90
4	DIPEA[41]	$CHCl_3$/ 0 °C	45 h	90
5	L-proline-linked N-GQDs/ZnO/CuO [Our Job]	EtOH/ reflux	45 min	96

[a] Reaction conditions: 4-nitrobenzaldehyde (1 mmol), 4-hydroxycoumarin (1 mmol), and phenacyl bromide (1 mmol).
[b] Isolated yield.

Table 4. Diastereoselective synthesis of furocoumarins utilizing L-proline-linked N-GQDs/ZnO/CuO nanocomposites under reflux conditions.

No.	R	Product	Diastereomeric ratio of product (*trans: cis*)[a]	Time (min)	Yield (%)[b]
1	H	5a	60:40	55	94
2	4-NO₂	5b	93:7	45	96
3	4-Cl	5c	70:30	55	95
4	2-Cl	5d	67:33	65	94
5	4-Br	5e	70:30	55	94
6	2-F	5f	87:13	60	93
7	4-SCH₃	5g	66:34	80	90
8	4-OMe	5h	64:36	85	87
9	4-Me	5i	61:39	75	89
10	4-OH	5j	62:38	80	86
11	3-Me	5k	61:39	80	89
12	3-F	5l	85:15	60	95
13	3-NO2	5m	93:7	50	96

[a] Determined on the crude reaction mixture by ¹H NMR
[b] isolated yield

active site) can have an outstanding effective impact on diastereoisomer formation, reaction time, energy usage, and green solvent usage. Consequently, studied of results published and comparison with our catalyst, it can be said that L-proline-linked N-GQDs/ZnO/CuO as a chiral retrievable metal-organocatalyst play the main role in diastereoselectivity of reaction. According to this one-pot protocol, various furocoumarins were synthesized. Inspired by furocoumarins stereochemistry and using the optimized reaction conditions, we investigated the preparation of a category of furo[3,2-*c*]coumarins base on stereoisomer formation in one-pot domino reactions using various aromatic aldehydes (Table 4).

From a comparison of various aryl aldehydes with electron-withdrawing groups and electron-releasing groups, it appeared that aromatic aldehydes with electron-withdrawing groups reacted quickly. To improve our comprehensive of stereoselectivity, we have proposed a plausible reaction mechanism for the formation of furo[3,2-c]coumarins in attendance of ZnO/CuO@N-GQDs@L-proline heterojunction nanocomposites which is shown in Fig. 13.

In this instance, pyridine **(3)** and phenacyl bromide **(4)** (in a 1:1 mole ratio) were firstly mixed for 1 min to form the (cyanomethyl) pyridinium bromide salt through an S_N2 reaction. Afterward, aryl aldehyde **(1)**, 4-hydroxycoumarin **(2)**, and chiral nanocatalyst were added to the above mixture and heated at reflux conditions for an appropriate time. In the presence of chiral organometallic nanocatalyst, the reaction starts via Knoevenagel condensation between aromatic aldehyde and 4-hydroxycoumarin to form intermediate **(I)**. In this part, presumably modified L-proline plays two roles: (i) basic catalytic role (shown in blue) to abstract the proton from 4- hydroxycoumarin **2** and a proton from the 1-(4-bromophenyl)-2-pyridinium **5** (ii) electrostatic interaction role (shown in red) to activation of carbonyl of aryl aldehyde **1**. Next, the Michael addition of the in situ prepared pyridinium ylide to intermediate **(I)** affords the intermediate **(II)**. According to the
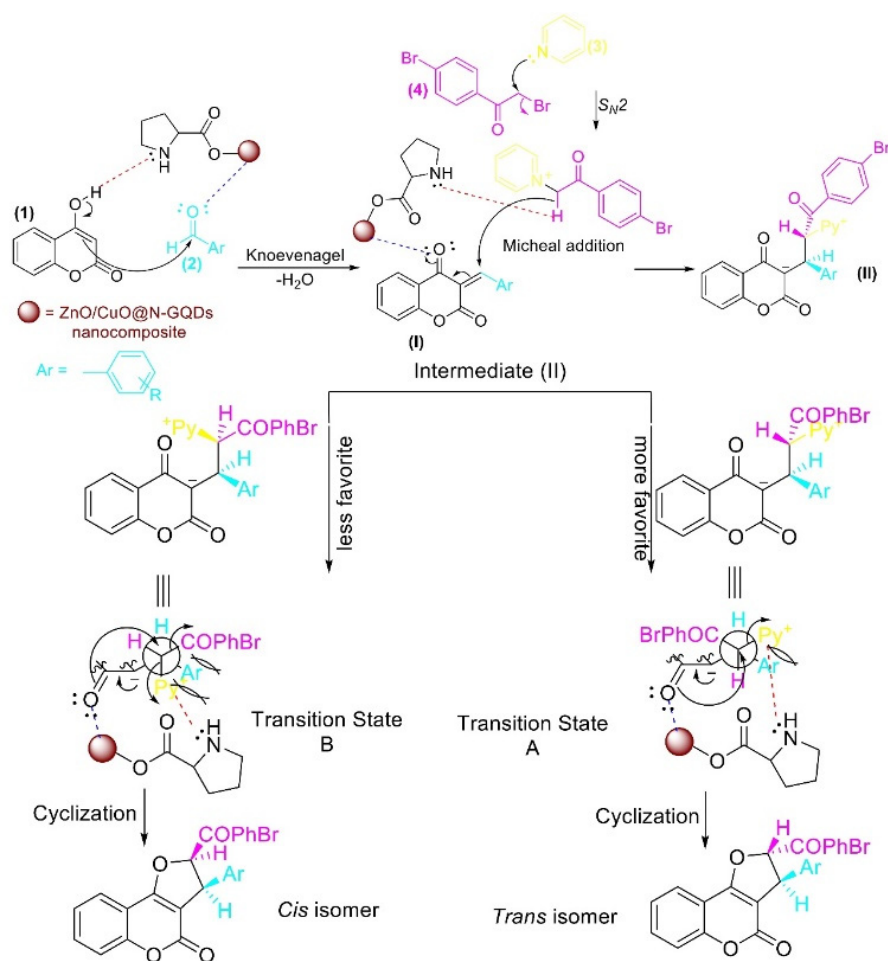
Fig. 13. Mechanistic proposal for diastereoselective synthesis of furocoumarins in attendance of L-proline-linked N-GQDs/ZnO/CuO heterojunction nanocomposites.

previously reported [41], despite the existence of three nucleophilic centers for the continuation of the reaction, it is done only by removing the pyridinium group (path shown). The main point in the stereochemistry of products is that the diastereoselectivity of reaction is influenced by the interaction of intermediate (**II**) with the chiral catalyst in transition states A and B.

As illustrated in Fig. 13, there is only gauche interaction between pyridinium (leaving group) and aromatic aldehyde which is followed by a nucleophilic enolate attack from the backside of the electrophilic carbon atom bearing the pyridinium group. Therefore, the major product obtained is *trans* [52]. *Cis*-product is a miner isomer due to two severe steric repulsions which can be observed in transition state B and in itself. The structure of isolated *trans*-2-benzoyl-3-(aryl)-2H-

furo[3,2-c]chromen-4(3H)-ones were completely identified by ^{1}H and ^{13}C NMR spectroscopic data, FT-IR spectra data, and CHNS analysis. For instance, in the ^{1}H NMR spectrum of 5b, two protons at 2 and 3 positions of dihydrofuran appeared as two doublets signal at 5.13 and 6.05 ppm with the vicinal coupling constant J = 5.6 Hz. A similar signal in the ^{1}H NMR spectrum was also observed at 5.30 and 5.94 ppm with the vicinal coupling constant J = 8 Hz (Fig. 14). It is found that the vicinal coupling constant of two methine protons in *trans* isomer in 5-membered rings appeared with J = 4-7 Hz, whereas, in the case of *cis*-isomer this coupling constant appeared with J = 7-10 Hz [44, 53, 54]. The structure of stereochemistry was confirmed by X-ray analysis which was accomplished on 5f and showed that the two protons at 2 and 3 positions of dihydrofuran existed in the *trans*
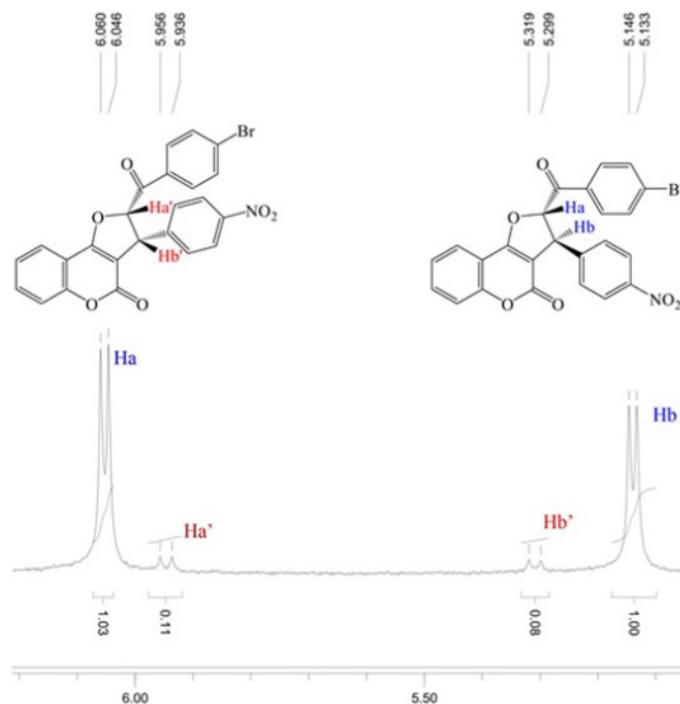
Fig. 14. ^{1}H NMR spectrum of 5b.

Fig. 15. The X-ray crystal structure of 5f.
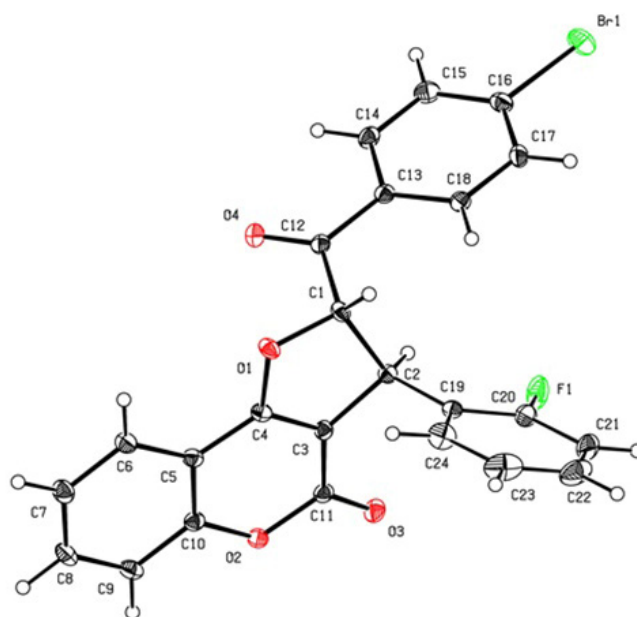
orientation (Fig. 15). By comparing the previous reports[39-44], in this method, the L-proline-linked N-GQDs/ZnO/CuO heterojunction nanocomposite was used as a chiral retrievable catalyst in the diastereoselective synthesis of furo[3,2-*c*] coumarins via one-pot multicomponent reactions to improve diastereoselectivity efficiency. As a result *cis*-isomer of furocoumarin, which has

Table 5. Recycling of nanocatalyst.

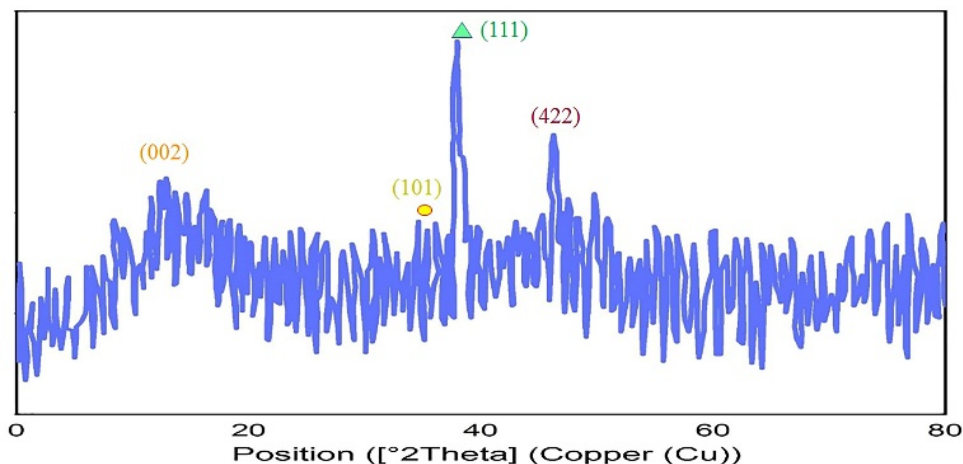| Test	1st	2nd	3rd	4th	5th	6th	7th
Yield (%)	96	96	94	93	91	87	81

Fig. 16. *XRD graph of L-proline-linked N-GQDs/ZnO/CuO nanocomposite after seven reaction runs.*

not been reported previously, was characterized in this research by ^{1}H NMR spectroscopy. Also, *trans*-isomer was determined by *X-ray* single crystallography, as well as the stereoselective synthesis of furo[3,2-*c*]coumarins in presence of chiral nanocatalyst, the products were prepared with high purity of *cis*-isomer.

Reusability of L-proline-linked N-GQDs/ZnO/CuO nanocomposites

Retrievability is one of the most outstanding issues among heterogeneous catalysts. The retrievability and reusability of L-proline-linked N-GQDs/ZnO/CuO nanocomposites are inspected after seven runs (model reaction, in optimized conditions). Upon completion of the reaction, separated nanocatalyst, washed with ethanol and deionized water at least 3 times, was left to dry and utilized with new substrates once more without excess purification. The results in Table 4 reveal the catalytic activity of nanocatalyst does not decline remarkably. According to the XRD graph (Fig. 16), the crystalline structure of reused catalyst was well preserved.

CONCLUSION

In this research, a straightforward procedure is proposed to form the L-proline-linked N-GQDs/ZnO/CuO nanocomposites. ZnO/CuO heterojunction nanostructure is directly generated using a highly controllable hydrothermal route. Especially, we investigated various techniques to analyze the catalytic execution of L-proline-linked N-GQDs/ZnO/CuO nanostructures and found that the L-proline-linked N-GQDs/CuO nanocomposites as a chiral retrievable catalyst had a considerable impact on the catalytic performance improvement. Also, we have described a diastereoselective Michael addition and intramolecular cyclization for the synthesis of *trans* furo[3,2-*c*]coumarins in the attendance of L-proline-linked N-GQDs/ZnO/CuO nanocatalyst. A proposed mechanism was suggested based on steric hindrance in the transition state. Briefly, this procedure allows the preparation of stereoisomers from the accessible precursors in an easy operation with excellent yields under environment-friendly conditions.

CONFLICT OF INTEREST

The authors declare that there is no conflict of interests regarding the publication of this manuscript.

REFERENCES

1. Yang J-S, Pai DZ, Chiang W-H. Microplasma-enhanced synthesis of colloidal graphene quantum dots at ambient conditions. Carbon. 2019;153:315-319.

2. Xi F, Zhao J, Shen C, He J, Chen J, Yan Y, et al. Amphiphilic graphene quantum dots as a new class of surfactants. Carbon. 2019;153:127-135.

3. Wen J, Xu Y, Li H, Lu A, Sun S. Recent applications of carbon nanomaterials in fluorescence biosensing and bioimaging. Chemical Communications. 2015;51(57):11346-11358.

4. Razmi H, Mohammad-Rezaei R. Graphene quantum dots as a new substrate for immobilization and direct electrochemistry of glucose oxidase: Application to sensitive glucose determination. Biosensors and Bioelectronics. 2013;41:498-504.

5. Zhang Y, He YH, Cui PP, Feng XT, Chen L, Yang YZ, et al. Water-soluble, nitrogen-doped fluorescent carbon dots for highly sensitive and selective detection of Hg2+ in aqueous solution. RSC Advances. 2015;5(50):40393-40401.

6. Mandani S, Sharma B, Dey D, Sarma TK. Carbon nanodots as ligand exchange probes in Au@C-dot nanobeacons for fluorescent turn-on detection of biothiols. Nanoscale. 2015;7(5):1802-1808.

7. Murugesan B, Pandiyan N, Arumugam M, Veerasingam M, Sonamuthu J, Jeyaraman AR, et al. Two dimensional graphene oxides converted to three dimensional P, N, F and B, N, F tri-doped graphene by ionic liquid for efficient catalytic performance. Carbon. 2019;151:53-67.

8. Purohit G, Kharkwal A, Rawat DS. CuIn-ethylxanthate, a "Versatile Precursor" for Photosensitization of Graphene-Quantum Dots and Nanocatalyzed Synthesis of Imidazopyridines with Ideal Green Chemistry Metrics. ACS Sustainable Chemistry & Engineering. 2020;8(14):5544-5557.

9. Chen J, Yu H, Tu D, Shen L. l-Proline functionalized metal-organic framework PCN-261 as catalyst for aldol reaction. Inorg Chem Commun. 2019;107:107448.

10. Roushani M, Shahdost-fard F. Applicability of AuNPs@N-GQDs nanocomposite in the modeling of the amplified electrochemical Ibuprofen aptasensing assay by monitoring of riboflavin. Bioelectrochemistry. 2019;126:38-47.

11. Sekar K, Raji G, Tong L, Zhu Y, Liu S, Xing R. Boosting the electrochemical performance of MoS2 nanospheres-N-doped-GQDs-rGO three-dimensional nanostructure for energy storage and conversion applications. Applied Surface Science. 2020;504:144441.

12. Kumar S, Dhiman A, Sudhagar P, Krishnan V. ZnO-graphene quantum dots heterojunctions for natural sunlight-driven photocatalytic environmental remediation. Applied Surface Science. 2018;447:802-815.

13. Xu Q, Ju D, Zhang Z, Yuan S, Zhang J, Xu H, et al. Near room-temperature triethylamine sensor constructed with CuO/ZnO P-N heterostructural nanorods directly on flat electrode. Sensors Actuators B: Chem. 2016;225:16-23.

14. Guo Q, Fu L, Yan T, Tian W, Ma D, Li J, et al. Improved photocatalytic activity of porous ZnO nanosheets by thermal deposition graphene-like g-C3N4 for CO2 reduction with H2O vapor. Applied Surface Science. 2020;509:144773.

15. Yu Z, Moussa H, Liu M, Schneider R, Moliere M, Liao H. Heterostructured metal oxides-ZnO nanorods films prepared by SPPS route for photodegradation applications.

16. Safaei-Ghomi J, Elyasi Z, Babaei P. N-doped graphene quantum dots modified with CuO (0D)/ZnO (1D) heterojunctions as a new nanocatalyst for the environmentally friendly one-pot synthesis of monospiro derivatives. New Journal of Chemistry. 2021.

17. Safaei-Ghomi J, Zahedi S. Diastereoselective synthesis of isoxazolidines and spiroisoxazolidines via catalytic 1,3-dipolar cycloaddition reactions in the presence of Fe3O4-l-proline nanoparticles as a magnetic organocatalyst. Tetrahedron Lett. 2016;57(10):1071-1073.

18. Luo S, Xu H, Mi X, Li J, Zheng X, Cheng J-P. Evolution of Pyrrolidine-Type Asymmetric Organocatalysts by "Click" Chemistry. The Journal of Organic Chemistry. 2006;71(24):9244-9247.

19. Chen G, Fu X, Li C, Wu C, Miao Q. Highly efficient direct a larger-scale aldol reactions catalyzed by a flexible prolinamide based-metal Lewis acid bifunctional catalyst in the presence of water. J Organomet Chem. 2012;702:19-26.

20. Tan R, Li C, Luo J, Kong Y, Zheng W, Yin D. An effective heterogeneous l-proline catalyst for the direct asymmetric aldol reaction using graphene oxide as support. Journal of Catalysis. 2013;298:138-147.

21. Hajizadeh Z, Maleki A. Poly(ethylene imine)-modified magnetic halloysite nanotubes: A novel, efficient and recyclable catalyst for the synthesis of dihydropyrano[2,3-c] pyrazole derivatives. Molecular Catalysis. 2018;460:87-93.

22. Nagaraju S, Paplal B, Sathish K, Giri S, Kashinath D. Synthesis of functionalized chromene and spirochromenes using l-proline-melamine as highly efficient and recyclable homogeneous catalyst at room temperature. Tetrahedron Lett. 2017;58(44):4200-4204.

23. Xu L, Wang F, Huang J, Yang C, Yu L, Fan Y. l-Proline and thiourea co-catalyzed condensation of acetone. Tetrahedron. 2016;72(27):4076-4080.

24. Yu L, Luan J, Xu L, Ding Y, Xu Q. Proline and secondary amine co-catalyzed condensation of cyclobutanone with aldehydes: a facile access to 2-methylenecyclobutanones under near neutral conditions. Tetrahedron Lett. 2015;56(44):6116-6119.

25. Zou J, Zhao W, Li R, Zhang H, Cui Y. Synthesis of PVC-TEPA-supported proline derivative and its catalytic behavior in the direct asymmetric aldol reaction. J Appl Polym Sci. 2010;118(2):1020-1026.

26. Doyagüez EG, Calderón F, Sánchez F, Fernández-Mayoralas A. Asymmetric Aldol Reaction Catalyzed by a Heterogenized Proline on a Mesoporous Support. The Role of the Nature of Solvents. The Journal of Organic Chemistry. 2007;72(24):9353-9356.

27. Luo S, Mi X, Zhang L, Liu S, Xu H, Cheng J-P. Functionalized Chiral Ionic Liquids as Highly Efficient Asymmetric Organocatalysts for Michael Addition to Nitroolefins. Angew Chem Int Ed. 2006;45(19):3093-3097.

28. Kutzscher C, Nickerl G, Senkovska I, Bon V, Kaskel S. Proline Functionalized UiO-67 and UiO-68 Type Metal–Organic Frameworks Showing Reversed Diastereoselectivity in Aldol Addition Reactions. Chem Mater. 2016;28(8):2573-2580.

29. Nguyen KD, Kutzscher C, Drache F, Senkovska I, Kaskel S. Chiral Functionalization of a Zirconium Metal–Organic Framework (DUT-67) as a Heterogeneous Catalyst in Asymmetric Michael Addition Reaction. Inorganic

Chemistry. 2018;57(3):1483-1489.

30. Zamboulis A, Rahier NJ, Gehringer M, Cattoën X, Niel G, Bied C, et al. Silica-supported l-proline organocatalysts for asymmetric aldolisation. Tetrahedron: Asymmetry. 2009;20(24):2880-2885.

31. Mecadon H, Rohman MR, Kharbangar I, Laloo BM, Kharkongor I, Rajbangshi M, et al. l-Proline as an efficient catalyst for the multi-component synthesis of 6-amino-4-alkyl/aryl-3-methyl-2,4-dihydropyrano[2,3-c]pyrazole-5-carbonitriles in water. Tetrahedron Lett. 2011;52(25):3228-3231.

32. Xie J-W, Li P, Wang T, Zhou F-T. Efficient and mild synthesis of functionalized 2,3-dihydrofuran derivatives via domino reaction in water. Tetrahedron Lett. 2011;52(18):2379-2382.

33. Sardari S, Mori Y, Horita K, Micetich RG, Nishibe S, Daneshtalab M. Synthesis and antifungal activity of coumarins and angular furanocoumarins. Biorg Med Chem. 1999;7(9):1933-1940.

34. Rajabi M, Hossaini Z, Khalilzadeh MA, Datta S, Halder M, Mousa SA. Synthesis of a new class of furo[3,2-c]coumarins and its anticancer activity. J Photochem Photobiol B: Biol. 2015;148:66-72.

35. Campos-Toimil M, Orallo F, Santana L, Uriarte E. Synthesis and Vasorelaxant Activity of New Coumarin and Furocoumarin Derivatives. Bioorg Med Chem Lett. 2002;12(5):783-786.

36. Girennavar B, Poulose SM, Jayaprakasha GK, Bhat NG, Patil BS. Furocoumarins from grapefruit juice and their effect on human CYP 3A4 and CYP 1B1 isoenzymes. Biorg Med Chem. 2006;14(8):2606-2612.

37. Olomola TO, Mosebi S, Klein R, Traut-Johnstone T, Coates J, Hewer R, et al. Novel furocoumarins as potential HIV-1 integrase inhibitors. Bioorg Chem. 2014;57:1-4.

38. Rozhkov RV, Larock RC. Synthesis of Dihydrofurocoumarins via Palladium-Catalyzed Annulation of 1,3-Dienes by o-Iodoacetoxycoumarins. Org Lett. 2003;5(6):797-800.

39. Karanjule N, Samant S. Microwave Assisted, 4-dimethylaminopyridine (DMAP) Mediated, Onepot, Three-component, Regio- and Diastereoselective Synthesis of Trans- 2,3-dihydrofuro[3,2-c]coumarins. Current Microwave Chemistry. 2014;1:135-141.

40. Altieri E, Cordaro M, Grassi G, Risitano F, Scala A. Regio and diastereoselective synthesis of functionalized 2,3-dihydrofuro[3,2-c]coumarins via a one-pot three-component reaction. Tetrahedron. 2010;66(49):9493-9496.

41. Rajesh SM, Perumal S, Menéndez JC, Pandian S, Murugesan R. Facile ionic liquid-mediated, three-component sequential reactions for the green, regio- and diastereoselective synthesis of furocoumarins. Tetrahedron. 2012;68(27):5631-5636.

42. Tan X-c, Zhao H-y, Pan Y-m, Wu N, Wang H-s, Chen Z-f. Atom-economical chemoselective synthesis of furocoumarins via cascade palladium catalyzed oxidative alkoxylation of 4-oxohydrocoumarins and alkenes. RSC Advances. 2015;5(7):4972-4975.

43. Zareai Z, Khoobi M, Ramazani A, Foroumadi A, Souldozi A, Ślepokura K, et al. Synthesis of functionalized furo[3,2-c] coumarins via a one-pot oxidative pseudo three-component reaction in poly(ethylene glycol). Tetrahedron. 2012;68(33):6721-6726.

44. Wang Q-F, Hou H, Hui L, Yan C-G. Diastereoselective Synthesis of trans-2,3-Dihydrofurans with Pyridinium Ylide Assisted Tandem Reaction. The Journal of Organic Chemistry. 2009;74(19):7403-7406.

45. Qiu Z, Han X, Li M, Wang Y, Chen X, Fan W, et al. The temporal variability of hydrothermal activity of Wocan hydrothermal field, Carlsberg Ridge, northwest Indian Ocean. Ore Geology Reviews. 2021:103999.

46. Safardoust-Hojaghan H, Salavati-Niasari M, Amiri O, Rashki S, Ashrafi M. Green synthesis, characterization and antimicrobial activity of carbon quantum dots-decorated ZnO nanoparticles. Ceram Int. 2021;47(4):5187-5197.

47. Cao L, Wang X, Meziani MJ, Lu F, Wang H, Luo PG, et al. J Am Chem Soc. 2007;129:11318.

48. Kharmawlong GK, Nongrum R, Chhetri B, Rani JWS, Rahman N, Yadav AK, et al. Green and efficient one-pot synthesis of 2,3-dihydroquinazolin-4(1H)-ones and their anthelmintic studies. Synth Commun. 2019;49(20):2683-2695.

49. Cheng W, Pan J, Yang J, Zheng Z, Lu F, Chen Y, et al. A photoelectrochemical aptasensor for thrombin based on the use of carbon quantum dot-sensitized TiO2 and visible-light photoelectrochemical activity. Microchimica Acta. 2018;185(5):263.

50. Safaei-Ghomi J, Pooramiri P, Babaei P. Green sonosynthesis of phenazinpyrimidines using Co3O4/ZnO@N-GQDs@ SO3H nanocomposite as a robust heterogeneous catalyst. J Chin Chem Soc. 2021;n/a(n/a).

51. Son DI, Kwon BW, Park DH, Seo W-S, Yi Y, Angadi B, et al. Emissive ZnO–graphene quantum dots for white-light-emitting diodes. Nature Nanotechnology. 2012;7(7):465-471.

52. Soejima T, Satoh K, Kamigaito M. Control of stereochemistry in atom transfer radical addition and step-growth radical polymerization by chiral transition metal catalysts. Tetrahedron. 2016;72(48):7657-7664.

53. Kumar A, Srivastava S, Gupta G. Cascade [4 + 1] annulation via more environmentally friendly nitrogen ylides in water: synthesis of bicyclic and tricyclic fused dihydrofurans. Green Chem. 2012;14(12):3269-3272.

54. Adamo M, Suresh S, Piras L. Tetrahedron. 2009;65:5402.

55. Tangella Y, Manasa KL, Laxma Nayak V, Sathish M, Sridhar B, Alarifi A, et al. An efficient one-pot approach for the regio- and diastereoselective synthesis of trans-dihydrofuran derivatives: cytotoxicity and DNA-binding studies. Org Biomol Chem. 2017;15(32):6837-6853.

56. Fan L-P, Li P, Li X-S, Xu D-C, Ge M-M, Zhu W-D, et al. Facile Domino Access to Chiral Mono-, Bi-, and Tricyclic 2,3-Dihydrofurans. The Journal of Organic Chemistry. 2010;75(24):8716-8719.